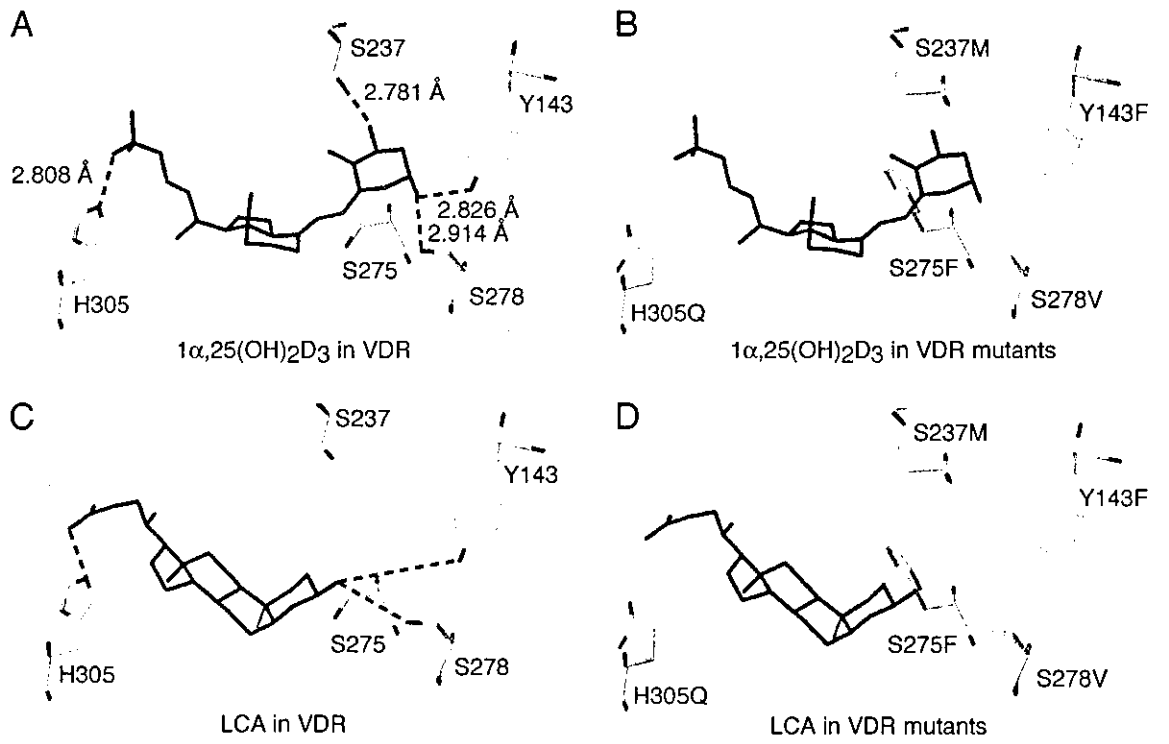

Fig. 5. Molecular Modeling of VDR Interaction Within Ligands

A, Amino acid residues forming hydrogen bonds with $1\alpha,25(OH)_2D_3$. 25-Hydroxyl group, 1α-hydroxyl group, and 3-hydroxyl group of $1\alpha,25(OH)_2D_3$ make hydrogen bonds with H305, S237, and Y143/S278 of VDR, respectively. B, Docking model of VDR point mutants with $1\alpha,25(OH)_2D_3$. S237M and S275F mutations are predicted to weaken interaction with $1\alpha,25(OH)_2D_3$, whereas the effects of H305Q, Y143F, and S278V on the modeled interaction are minor. C, Docking model of LCA and wild-type VDR. Y143 and S278 weakly interact with the 3-hydroxyl group of LCA. These interactions are critical because S237 cannot hydrogen bond with LCA. H305 is suitably positioned to form a hydrogen bond with the carboxyl group of LCA. D, Docking model of LCA and VDR mutants. Mutation of S278V, H305Q, and S275F would be expected to destabilize interaction with LCA. Because S237 does not interact with LCA, S237M would be expected to have no effect on LCA interaction.

defects in bile acid response with normal calcium metabolism whereas VDR-S237M-expressing mice may show selective dysfunction in vitamin D response. Development of ligand-specific VDR-substituted mice should provide a valuable tool in clarifying VDR function *in vivo*.

MATERIALS AND METHODS

Chemical Compounds

$1\alpha,25(OH)_2D_3$ and LCA were obtained from Calbiochem (San Diego, CA) and Nacalai (Kyoto, Japan), respectively.

Graphical Manipulation and Docking

Graphical manipulations were performed using SYBYL 6.7 (Tripos, St. Louis, MO) (6, 31). The atomic coordinates of the crystal structures of hVDR-LBD (Δ165–215) (1DB1) and hPXR-LBD (1ILH) were retrieved from the Protein Data Bank. LCA was docked into VDR and PXR using the docking software FlexX (version 1.11.0; Tripos). The active site (in the case of NRs, the LBP) was defined to include all amino acids within 6.5 Å of the cocrystallized ligand.

Plasmids

A fragment of hVDR (GenBank accession no. J03258) was inserted into pCMX-flag vector to make pCMX-VDR (10, 32). The LBD of hVDR was inserted into pCMX-GAL4 vector to make pCMX-GAL4-VDR, and full-length hVDR was inserted into pCMX-VP16 vector to make pCMX-VP16-VDR (10). Nuclear hormone receptor-interacting domains of SRC-1 (amino acids 595–771; GenBank accession no. U90661) and N-CoR (1990–2416; GenBank accession no. U35312) were inserted into pCMX-GAL4 vector for pCMX-GAL4-SRC-1 and pCMX-GAL4-N-CoR, respectively. Mutations were introduced into pCMX-VDR, pCMX-GAL4-VDR, and pCMX-VP16-VDR using QuikChange Site-Directed Mutagenesis Kit (Stratagene, La Jolla, CA). VDR-responsive hCYP3A4-ER-6x3-tk-LUC and GAL4-responsive MH100(UAS)x4-tk-LUC reporters were used (10, 32). All plasmids were sequenced before use to verify DNA sequence fidelity.

Cell Culture and Cotransfection Assay

Human embryonic kidney HEK293 cells were cultured in DMEM containing 5% fetal bovine serum and antibiotic-antimycotic (Nacalai) at 37 C in a humidified atmosphere of 5% CO_2 in air. Transfections were performed by the calcium phosphate coprecipitation assay as previously described (33). Eight hours after transfection, ligands were added. Cells were harvested approximately 16–20 h after the treatment,

and luciferase and β-galactosidase activities were assayed using a luminometer and a microplate reader (Molecular Devices, Sunnyvale, CA). DNA cotransfection experiments included 50 ng reporter plasmid, 20 ng pCMX-β-galactosidase, 15 ng of each receptor and/or cofactor expression plasmid, and pGEM carrier DNA for a total of 150 ng DNA per well in a 96-well plate. Luciferase data were normalized to an internal β-galactosidase control and represent the mean (±SD) of triplicate assays.

Ligand-Binding Assay

LBDs of hVDR and its mutants were cloned into the GST-fusion vector pGEX-4T1 (Amersham Pharmacia Biotech, Piscataway, NJ). GST-VDR fusion proteins were expressed in BL21 DE3 cells (Promega Corp., Madison, WI) and purified with glutathione sepharose beads (Amersham Pharmacia Biotech). Competitive ligand-binding assay was performed by modification of previous reports (34, 35). Briefly, 500 ng GST fusion proteins were bound to glutathione sepharose and incubated with [26,27-methyl-^{3}H]1α,25$(OH)_2D_3$ (Amersham Pharmacia Biotech) in the presence or absence of nonradioactive ligand in a buffer (10 mM Tris-HCl, pH 7.6; 1 mM EDTA; 300 mM KCl; 1 mM dithiothreitol; 10% glycerol) for 3 h at 4 C. After washing twice, the protein and bound 1α,25$(OH)_2D_3$ were resuspended in 200 μl of the binding buffer, and 150 μl were assessed by liquid scintillation counting.

Acknowledgments

We thank N. Mahmood, E. Kaneko, K. Morita, and H. Nakano for assistance in preparing plasmids and members of the Mangelsdorf, Shimomura, Makishima, and Yamada laboratories for helpful comments.

Received June 24, 2003. Accepted September 22, 2003.

Address all correspondence and requests for reprints to: Makoto Makishima, Graduate School of Frontier Biosciences, Osaka University, 2–2 Yamadaoka, H2, Suita, Osaka 565-0871, Japan. E-mail: maxima@fbs.osaka-u.ac.jp.

This work was supported by the Howard Hughes Medical Institute, the Robert A. Welch Foundation (D.J.M.), NIH Grant U19-DK62463 (D.J.M.), the Ministry of Health, Labor and Welfare, Japan (M.M.), the Ministry of Education, Culture, Sports, Science and Technology, Japan (M.M.), Yakult Bioscience Research Foundation (M.M.), and a Pharmacological Sciences training grant from the National Institutes of Health (A.I.S.). D.J.M. is an investigator and M.M. was an associate (until March 2002) of the Howard Hughes Medical Institute.

REFERENCES

1. Mangelsdorf DJ, Thummel C, Beato M, Herrlich P, Schutz G, Umesono K, Blumberg B, Kastner P, Mark M, Chambon P, Evans RM 1995 The nuclear receptor superfamily: the second decade. Cell 83:835–839
2. Glass CK, Rosenfeld MG 2000 The coregulator exchange in transcriptional functions of nuclear receptors. Genes Dev 14:121–141
3. Bouillon R, Okamura WH, Norman AW 1995 Structure-function relationships in the vitamin D endocrine system. Endocr Rev 16:200–257
4. Haussler MR, Whitfield GK, Haussler CA, Hsieh JC, Thompson PD, Selznick SH, Dominguez CE, Jurutka PW 1998 The nuclear vitamin D receptor: biological and molecular regulatory properties revealed. J Bone Miner Res 13:325–349
5. Yamada S, Shimizu M, Yamamoto K 2003 Structure-function relationships of vitamin D including ligand recognition by the vitamin D receptor. Med Res Rev 23: 89–115
6. Yamamoto K, Masuno H, Choi M, Nakashima K, Taga T, Ooizumi H, Umesono K, Sicinska W, VanHooke J, DeLuca HF, Yamada S 2000 Three-dimensional modeling of and ligand docking to vitamin D receptor ligand binding domain. Proc Natl Acad Sci USA 97:1467–1472
7. Norman AW, Adams D, Collins ED, Okamura WH, Flettterick RJ 1999 Three-dimensional model of the ligand binding domain of the nuclear receptor for 1α,25-dihydroxy-vitamin D_3. J Cell Biochem 74:323–333
8. Rochel N, Wurtz JM, Mitschler A, Klaholz B, Moras D 2000 The crystal structure of the nuclear receptor for vitamin D bound to its natural ligand. Mol Cell 5:173–179
9. Norman AW, Ishizuka S, Okamura WH 2001 Ligands for the vitamin D endocrine system: different shapes function as agonists and antagonists for genomic and rapid response receptors or as a ligand for the plasma vitamin D binding protein. J Steroid Biochem Mol Biol 76:49–59
10. Makishima M, Lu TT, Xie W, Whitfield GK, Domoto H, Evans RM, Haussler MR, Mangelsdorf DJ 2002 Vitamin D receptor as an intestinal bile acid sensor. Science 296: 1313–1316
11. Nagengast FM, Grubben MJ, van Munster IP 1995 Role of bile acids in colorectal carcinogenesis. Eur J Cancer 31A:1067–1070
12. Makishima M, Okamoto AY, Repa JJ, Tu H, Learned RM, Luk A, Hull MV, Lustig KD, Mangelsdorf DJ, Shan B 1999 Identification of a nuclear receptor for bile acids. Science 284:1362–1365
13. Parks DJ, Blanchard SG, Bledsoe RK, Chandra G, Consler TG, Kliewer SA, Stimmel JB, Willson TM, Zavacki AM, Moore DD, Lehmann JM 1999 Bile acids: natural ligands for an orphan nuclear receptor. Science 284: 1365–1368
14. Wang H, Chen J, Hollister K, Sowers LC, Forman BM 1999 Endogenous bile acids are ligands for the nuclear receptor FXR/BAR. Mol Cell 3:543–553
15. Staudinger JL, Goodwin B, Jones SA, Hawkins-Brown D, MacKenzie KI, LaTour A, Liu Y, Klaassen CD, Brown KK, Reinhard J, Willson TM, Koller BH, Kliewer SA 2001 The nuclear receptor PXR is a lithocholic acid sensor that protects against liver toxicity. Proc Natl Acad Sci USA 98:3369–3374
16. Xie W, Radominska-Pandya A, Shi Y, Simon CM, Nelson MC, Ong ES, Waxman DJ, Evans RM 2001 An essential role for nuclear receptors SXR/PXR in detoxification of cholestatic bile acids. Proc Natl Acad Sci USA 98: 3375–3380
17. Lehmann JM, McKee DD, Watson MA, Willson TM, Moore JT, Kliewer SA 1998 The human orphan nuclear receptor PXR is activated by compounds that regulate CYP3A4 gene expression and cause drug interactions. J Clin Invest 102:1016–1023
18. Blumberg B, Sabbagh Jr W, Juguilon H, Bolado Jr J, van Meter CM, Ong ES, Evans RM 1998 SXR, a novel steroid and xenobiotic-sensing nuclear receptor. Genes Dev 12: 3195–3205
19. Watkins RE, Wisely GB, Moore LB, Collins JL, Lambert MH, Williams SP, Willson TM, Kliewer SA, Redinbo MR 2001 The human nuclear xenobiotic receptor PXR: structural determinants of directed promiscuity. Science 292: 2329–2333
20. Takada I, Yu RT, Xu HE, Lambert MH, Montana VG, Kliewer SA, Evans RM, Umesono K 2000 Alteration of a single amino acid in peroxisome proliferator-activated receptor-α (PPARα) generates a PPARδ phenotype. Mol Endocrinol 14:733–740
21. Greschik H, Wurtz JM, Sanglier S, Bourguet W, van Dorsselaer A, Moras D, Renaud JP 2002 Structural and functional evidence for ligand-independent transcrip-

tional activation by the estrogen-related receptor 3. Mol Cell 9:303–313
22. Choi M, Yamamoto K, Itoh T, Makishima M, Mangelsdorf DJ, Moras D, DeLuca HF, Yamada S 2003 Interaction between vitamin D receptor and vitamin D ligands: two-dimensional alanine scanning mutational analysis. Chem Biol 10:261–270
23. Rochel N, Tocchini-Valentini G, Egea PF, Juntunen K, Garnier JM, Vihko P, Moras D 2001 Functional and structural characterization of the insertion region in the ligand binding domain of the vitamin D nuclear receptor. Eur J Biochem 268:971–979
24. Maglich JM, Sluder A, Guan X, Shi Y, McKee DD, Carrick K, Kamdar K, Willson TM, Moore JT 2001 Comparison of complete nuclear receptor sets from the human, *Caenorhabditis elegans* and *Drosophila* genomes. Genome Biol 2:RESEARCH0029
25. Moore LB, Maglich JM, McKee DD, Wisely B, Willson TM, Kliewer SA, Lambert MH, Moore JT 2002 Pregnane X receptor (PXR), constitutive androstane receptor (CAR), and benzoate X receptor (BXR) define three pharmacologically distinct classes of nuclear receptors. Mol Endocrinol 16:977–986
26. Dussault I, Lin M, Hollister K, Fan M, Termini J, Sherman MA, Forman BM 2002 A structural model of the constitutive androstane receptor defines novel interactions that mediate ligand-independent activity. Mol Cell Biol 22: 5270–5280
27. Xie W, Barwick JL, Simon CM, Pierce AM, Safe S, Blumberg B, Guzelian PS, Evans RM 2000 Reciprocal activation of xenobiotic response genes by nuclear receptors SXR/PXR and CAR. Genes Dev 14:3014–3023
28. Takeyama K, Masuhiro Y, Fuse H, Endoh H, Murayama A, Kitanaka S, Suzawa M, Yanagisawa J, Kato S 1999 Selective interaction of vitamin D receptor with transcriptional coactivators by a vitamin D analog. Mol Cell Biol 19:1049–1055
29. Xie W, Barwick JL, Downes M, Blumberg B, Simon CM, Nelson MC, Neuschwander-Tetri BA, Brunt EM, Guzelian PS, Evans RM 2000 Humanized xenobiotic response in mice expressing nuclear receptor SXR. Nature 406: 435–439
30. Zhang J, Huang W, Chua SS, Wei P, Moore DD 2002 Modulation of acetaminophen-induced hepatotoxicity by the xenobiotic receptor CAR. Science 298:422–424
31. Choi M, Yamamoto K, Masuno H, Nakashima K, Taga T, Yamada S 2001 Ligand recognition by the vitamin D receptor. Bioorg Med Chem 9:1721–1730
32. Willy PJ, Mangelsdorf DJ 1997 Unique requirements for retinoid-dependent transcriptional activation by the orphan receptor LXR. Genes Dev 11:289–298
33. Lu TT, Makishima M, Repa JJ, Schoonjans K, Kerr TA, Auwerx J, Mangelsdorf DJ 2000 Molecular basis for feedback regulation of bile acid synthesis by nuclear receptors. Mol Cell 6:507–515
34. Nakajima S, Hsieh JC, MacDonald PN, Galligan MA, Haussler CA, Whitfield GK, Haussler MR 1994 The C-terminal region of the vitamin D receptor is essential to form a complex with a receptor auxiliary factor required for high affinity binding to the vitamin D-responsive element. Mol Endocrinol 8:159–172
35. Solomon C, Macoritto M, Gao XL, White JH, Kremer R 2001 The unique tryptophan residue of the vitamin D receptor is critical for ligand binding and transcriptional activation. J Bone Miner Res 16:39–45

Molecular Endocrinology **is published monthly by The Endocrine Society (http://www.endo-society.org), the foremost professional society serving the endocrine community.**

0013-7227/03/$15.00/0
Printed in U.S.A.

The Journal of Clinical Endocrinology & Metabolism 88(5):2250–2255

doi: 10.1210/jc.2002-021610

Plasma Levels of Parathyroid Hormone (1–84) Whole Molecule and Parathyroid Hormone (7–84)-Like Fragments in Pseudohypoparathyroidism Type I

YURIKO HATAKEYAMA, KAZUTOSHI MIZUNASHI, YOHTARO FURUKAWA, SHIGEMITSU YABUKI, YUMI SATO, AND TERUO IGARASHI

Division of Laboratory Medicine (Y.H., S.Y., Y.S., T.I.), Tohoku University School of Medicine, Aoba-ku, Sendai 980-8574; Department of Internal Medicine (K.M.), Senen General Hospital, Tagajo 985-0842; and Sendai Open Hospital (Y.F.), Miyagino-ku, Sendai 984-0814, Japan

PTH (7–84) has antagonistic effects on the calcemic and phosphaturic actions of PTH (1–84) whole molecule (bioPTH). Human plasma contains bioPTH and PTH (7–84)-like fragments. Using bioPTH-specific and nonspecific assays, we found that the patients with pseudohypoparathyroidism (PHP) type I with PTH-resistant hypocalcemia and hyperphosphatemia had the increased plasma levels of bioPTH and PTH (7–84)-like fragments than normal subjects (26.8 ± 13.2 *vs.* 2.37 ± 0.75 pmol/liter, $P < 0.01$ and 16.2 ± 8.8 *vs.* 0.82 ± 0.47 pmol/liter, $P < 0.01$, respectively). Calcitriol treatment increased phosphaturic response to PTH (1–34) ($P < 0.05$), and there was a negative correlation between phosphaturic response and the PTH levels ($P < 0.05$). These results suggested that the increased bioPTH and PTH (7–84)-like fragment levels may be related to the impaired phosphaturic response to PTH (1–34) in PHP type I. We also examined bioPTH-calcium dynamics in PHP type Ib patients and found that set-point calcium was 0.928 ± 0.045 mmol/liter and the baseline to maximal ratio of bioPTH was 0.96 ± 0.04. Calcitriol treatment increased set-point calcium to 1.129 ± 0.028 mmol/liter ($P < 0.01$) and suppressed baseline to maximal ratio of bioPTH to 0.35 ± 0.21 ($P < 0.01$). These bio-PTH calcium dynamics studies revealed the maximally stimulated baseline PTH secretion in PHP type Ib and demonstrated the effects of calcitriol on PTH-calcium curve shift and the degree of relative stimulation of baseline secretion. (*J Clin Endocrinol Metab* 88: 2250–2255, 2003)

PTH UNDERGOES EXTENSIVE proteolytic modifications after it is produced by the parathyroid glands. Therefore, human plasma contains PTH(1–84) whole molecule (bioPTH) and many other PTH fragments. Recently new assays that detect only bioPTH have been developed (1–4). Pseudohypoparathyroidism (PHP) type I is characterized by PTH-resistant hypocalcemia and secondary hyperparathyroidism. However, there were not any data on the circulating levels of bioPTH in PHP type I. In this study, we evaluated the bioPTH levels in this disorder using the bioPTH-specific assay.

PTH secretion is controlled mainly through the interaction of extracellular calcium (Ca) and Ca-sensing receptor of the parathyroid cells. PTH-Ca dynamic tests have been performed to examine the regulation of PTH release by Ca in human. However, there is a possibility that PTH measurements in the previous studies were complicated by the presence of inactive PTH fragments and the results did not accurately reflect the changes in PTH secretion from parathyroids. In this study, bioPTH-specific assay was used to analyze the PTH-Ca dynamics for the evaluation of PTH secretion in PHP type Ib patients before and after calcitriol treatment.

A recent study in rats demonstrated that PTH(7–84) has antagonistic effects on the calcemic and phosphaturic actions of PTH(1–84) (5). Human plasma contains PTH fragments that have the elution position of PTH(7–84) on high-performance liquid chromatography (3, 4). Therefore, there is a possibility that PTH(7–84)-like fragments modify the target organ response to PTH in PHP type I. Using bioPTH-specific assay and previous nonspecific assay, we examined the circulating levels of bioPTH and PTH(7–84)-like fragments in PHP type I and analyzed the relationship between the phosphaturic response to exogenous PTH(1–34) and plasma levels of these PTH fragments.

Abbreviations: bioPTH, PTH(1–84) whole molecule; B/M ratio, baseline PTH to maximum PTH ratio; Ca, calcium; iPTH, intact PTH(1–84) assay; PHP, pseudohypoparathyroidism.

Patients and Materials

PHP type I patients and normal subjects

Seven newly diagnosed patients with PHP type I (two patients with type Ia and five patients with type Ib) were studied (Table 1). The diagnosis of PHP was established by clinical symptoms along with hypocalcemia, hyperphosphatemia, high plasma levels of intact PTH, and reduced urinary cAMP and phosphate responses to iv infused human PTH(1–34) (121 pmol/kg weight), as described previously (6). The diagnosis of PHP type Ia was based on the presence of Albright's hereditary osteodystrophy and the heterozygous mutations in the GNAS1 gene. We found a heterozygous G→A substitution of the fifth base of intron 4 at the donor splice junction bordering the 3′ end of exon 4 in one patient and a heterozygous insertion of C at position 255 in exon 5 (gene accession M21741) in the other patient. These mutations produced a frame shift of the coding region and a premature stop codon. The PHP Ia patients had the increased TSH levels and the PHP Ib patients did not. EDTA plasma samples were collected before and after calcitriol treatment (1.5 μg/d). EDTA plasma samples were also collected from 53 apparently healthy, ambulatory, nonmedicated volunteers having normal plasma ionized calcium levels, plasma $1,25(OH)_2D$ levels, and serum creatinine levels. All samples were stored at −80C until analysis. Informed consent was obtained from all patients and normal individuals.

TABLE 1. Biochemical characteristics of the patients with PHP type I

	PHP Ia	PHP Ib	Normal subjects
Age	15.0 ± 2.8	25.4 ± 3.6	26.4 ± 10.0
Gender (M/F)	2/0	1/4	11/42
Plasma Ca^{++} (mmol/liter)	0.89 ± 0.01[a]	0.73 ± 0.08[a]	1.22 ± 0.04
Serum phosphate (mmol/liter)	2.34 ± 0.48[a]	1.62 ± 0.23[a]	1.18 ± 0.13
Plasma iPTH (pmol/liter)	46.4 ± 25.4[a]	40.1 ± 22.5[a]	3.1 ± 1.1
Plasma bioPTH (pmol/liter)			
Before calcitriol treatment	29.8 ± 16.4[a]	25.6 ± 13.8[a]	2.4 ± 0.8
After calcitriol treatment	4.0 ± 2.5	4.5 ± 2.9	
Serum creatinine (μmol/liter)	52.8 ± 8.8	61.6 ± 8.8	52.8 ± 8.8
Plasma $1,25(OH)_2D$ (pmol/liter)			
Before calcitriol treatment	66.8 ± 18.9	34.7 ± 9.5[a]	86.0 ± 17.0
After calcitriol treatment	108.0 ± 43.7	52.3 ± 9.1	
Plasma 25(OH)D (nmol/liter)	34.6 ± 2.3	37.6 ± 7.9	40.0 ± 0.7
Responses to PTH(1–34) infusion			
Before calcitriol treatment			
cAMP response (μmol/h)	0.064 ± 0.007	0.227 ± 0.146	
Phosphate response (mmol/2 h)	0.58 ± 0.06	0.83 ± 0.26	
After calcitriol treatment			
cAMP response (μmol/h)	0.220 ± 0.002	0.366 ± 0.215	
Phosphate response (mmol/2 h)	1.37 ± 0.226	1.10 ± 0.44	

Data are presented as mean ± SD. iPTH, Plasma PTH levels that were measured by luminometric Nichols Advantage Intact PTH (1–84) assay, which cross-reacts with both PTH(1–84) whole molecule (bioPTH) and PTH(7–84)-like fragments. Responses to iv infused human PTH(1–34) (121 pmol/kg weight) are presented as an increase in urinary excretion of cAMP and phosphate. The discriminative values of urinary cAMP and phosphate responses to PTH between PHP type I and PTH-deficient hypoparathyroidism were 1 μmol/h and 1.13 mmol/2 h, respectively. Multiplication factors to convert Systeme Internationale units to metric units are 9.424 for bioPTH and iPTH, 8.781 for PTH(7–84)-like fragments, 0.4187 for $1,25OHD_3$, 0.4006 for 25OHD, 0.0113 for creatinine, and 3.097 for phosphate.

[a] $P < 0.01$ *vs.* normal subjects.

Measurements

Plasma levels of bioPTH were determined by a two-site chemiluminescence immunoassay, Bio-intact PTH(1–84) assay (Nichols Institute, San Juan Capistrano, CA), that uses an acridinium ester-labeled goat anti-PTH antibody, which binds to the first five N-terminal amino acids of the human PTH molecule, and a biotinylated capture antibody recognizing the 39–84 region (3). The sandwich complex was bound to streptavidin-coated magnetic particles, incubated, and then washed. Thereafter the particles were quantitated in the luminometer. There was no cross-reactivity against PTH(2–34), (3–34), (4–34), or (5–34) peptides. The dose recovery was within 99.8–104%. The intra- and interassay variations were less than 3.0% and 3.6%, respectively. Normal ranges for bioPTH were 0.86–3.86 pmol/liter. Plasma PTH levels were also measured by luminometric Nichols Advantage intact PTH(1–84) assay (iPTH), which cross-reacts with both PTH(1–84) whole molecule and PTH(7–84)-like fragments. The intra- and interassay variations of this assay were less than 3.1% and 3.3%, respectively. Normal ranges for iPTH were 0.89–5.35 pmol/liter, respectively. Plasma concentrations of ionized Ca were measured using a NOVA Ca analyzer (Nova Biomedical, Waltham, MA). The normal range of plasma ionized Ca level was 1.050–1.275 mmol/liter. Plasma vitamin D metabolites were extracted by acetonitrile using Sep-Pak C-18 and purified by HPLC. Plasma levels of 25-hydroxyvitamin D and 1,25(OH)2D were determined by a competitive protein-binding assay using vitamin D depleted rat serum and radioreceptor assay using cytosol receptor, respectively (7).

In vivo *dynamic testing of PTH-Ca relationship*

PTH-Ca dynamic studies were performed in five patients with PHP type Ib. Stepwise changes of plasma Ca were produced by the graded infusions of citrate (anticoagulant-citrate-dextrose formula A containing per 100 ml: 2.45 g dextrose, 2.2 g sodium citrate, and 0.7 g citric acid) in the stimulation test or Ca gluconate in the inhibition test that were performed after an overnight fast as previously described (7). Blood samples for ionized Ca and PTH measurements were obtained anaerobically at the end of each step in citrate or Ca infusion protocol. From the data obtained during the inhibition and stimulation tests, the following parameters were defined: maximal PTH as the highest PTH level observed in response to hypocalcemia; the set point of calcium as the ionized Ca corresponding to the midpoint between the maximal PTH and minimal PTH; and the ratio of baseline PTH to maximal PTH that was the baseline PTH divided by the maximal PTH. We also evaluated the effects of calcitriol treatment (1.5 μg/d) on the sigmoidal PTH-Ca dynamics. The parameters of the sigmoidal curve were compared among three periods (before treatment, after 2 wk of treatment, and after 25 wk of treatment).

All results are presented as means ± SD. Differences among repeated measurements were analyzed by ANOVA, and the significance was assessed by Fisher's protected least significant difference test.

Results

Plasma levels of in PHP type I patients and normal individuals

The relationship between plasma bioPTH and ionized calcium in PHP type I is presented in Fig. 1. BioPTH levels were consistently lower than iPTH levels in PHP type I patients and normal subjects, and there was a linear correlation between bioPTH levels and iPTH levels (Fig. 2). The slope of the correlation curve and the bioPTH/iPTH ratio were lower in PHP type I patients than normal subjects (the bioPTH/iPTH ratio was 0.64 ± 0.03 in PHP type I patients before calcitriol treatment and 0.64 ± 0.07 in PHP type I patients after calcitriol treatment *vs.* 0.77 ± 0.06 in normal subjects, $P < 0.01$) (Fig. 3). The calculated levels of PTH(7–84)-like fragments (the values after subtracting bioPTH from iPTH) were higher in PHP type I patients than normal subjects [142.5 ± 76.9 pg/ml (16.2 ± 8.7 pmol/liter) *vs.* 7.2 ± 4.1 pg/ml (0.82 ± 0.47 pmol/liter), $P < 0.01$]. Calcitriol treatment suppressed the PTH(7–84)-like fragments levels to 24.0 ± 18.8 pg/ml (2.7 ± 2.1 pmol/liter) in these patients ($P < 0.01$ *vs.* before calcitriol treatment). The proportion of PTH(7–84)-like fragments to PTH(1–84) was higher in PHP type I patients than normal subjects (0.56 ± 0.07 in PHP type I patients before calcitriol

treatment and 0.58 ± 0.16 in PHP type I patients after calcitriol treatment *vs.* 0.30 ± 0.11 in normal subjects, $P < 0.01$).

The relationship between plasma PTH levels and phosphaturic response to exogenous PTH(1–34) in PHP type I patients

Phosphaturic response to exogenous PTH(1–34) [the increase in urinary phosphate excretion during 2 h after infusion of 121 pmol/kg weight PTH(1–34)] was 23.5 ± 7.7 mg (0.75 ± 0.24 mmol)/2 h in PHP type I patients before calcitriol treatment. The phosphaturic response increased to 36.3 ± 12.2 mg (1.17 ± 12.2 mmol)/2 h after calcitriol treatment ($P < 0.05$ *vs.* before calcitriol treatment). There was a negative correlation between the phosphaturic response and plasma PTH levels [PTH(1–84), $P < 0.05$ and PTH(7–84)-like fragments, $P < 0.05$] (Fig. 4). There was a slight increase in urinary cAMP responses after calcitriol treatment. However, there was not a significant statistical difference between before and after calcitriol treatment.

BioPTH-calcium dynamics in PHP type Ib

Bio PTH-Ca dynamics in five patients with PHP type Ib are summarized in Table 2 and Fig. 5. When the baseline calcium levels were low before calcitriol treatment, bioPTH concentrations responded to the changes in calcium at low calcium levels (set point: 0.928 ± 0.045 mmol/liter) (*coarse dashed line*). PTH dropped significantly after Ca infusion in the inhibition test. However, the further decrease in calcium, which was induced by citrate infusion in the stimulation test, produced

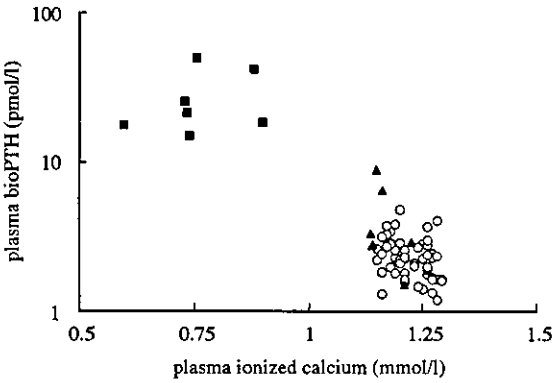

FIG. 1. The relationship between plasma PTH(1–84) whole-molecule and plasma ionized calcium in PHP type I. Plasma bioPTH levels were measured by Bio-intact PTH(1–84) assay in seven patients with PHP type I and 53 normal individuals. PHP type I patients before calcitriol treatment (■) had higher plasma PTH levels than normal individuals (○) ($P < 0.01$). PHP type I patients treated with 1.5 μg/d calcitriol had normal or slightly increased bioPTH levels (▲), which were lower than pretreatment values ($P < 0.01$ *vs.* before calcitriol treatment). There was a negative correlation between plasma bioPTH and plasma ionized Ca [plasma bioPTH (pmol/liter) = 60.4 + −46.6 × plasma ionized Ca (mmol/liter), r = 0.694, $P < 0.01$]. Multiplication factor to convert SI units to metric units is 9.424 for bioPTH.

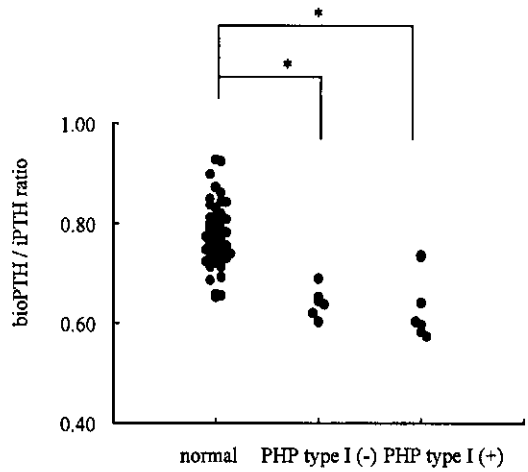

FIG. 3. The bioPTH/iPTH ratio in PHP type I patients and normal subjects. BioPTH/iPTH ratio was lower in PHP type I patients than normal subjects. PHP type I (−): PHP type I patients before calcitriol treatment. PHP type I (+): PHP type I patients after 1.5 μg/d calcitriol treatment. *, $P < 0.01$ *vs.* normal subjects.

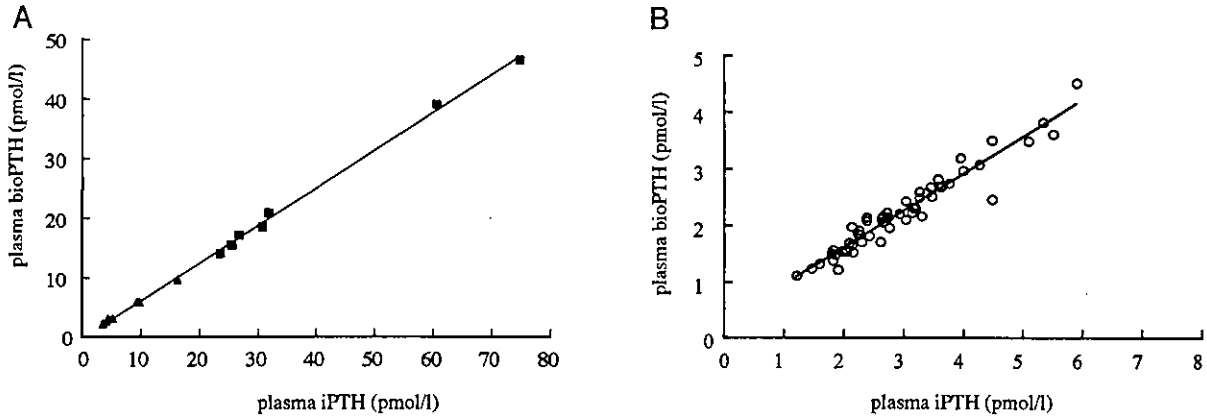

FIG. 2. The correlation between bioPTH and iPTH in PHP type I patients and normal subjects. Plasma bioPTH levels were compared with the iPTH levels that were measured by Nichols Advantage Intact PTH(1–84) assay, which cross-reacts with PTH(1–84) whole-molecule and PTH(7–84)-like fragments in seven patients with PHP type I (A) and 53 normal subjects (B) (■, PHP type I patients before calcitriol treatment; ▲, PHP type I patients after calcitriol treatment; ○, normal individuals). There was a linear correlation between bioPTH and iPTH levels. Plasma bioPTH (pmol/liter) = −0.888 + 0.587 × plasma iPTH (pmol/liter), r = 0.999 in PHP type I patients. Plasma bioPTH (pmol/liter) = 2.952 + 0.604 × plasma iPTH (pmol/liter), r = 0.965 in normal subjects. Multiplication factor to convert SI units to metric units is 9.424 for bioPTH and iPTH.

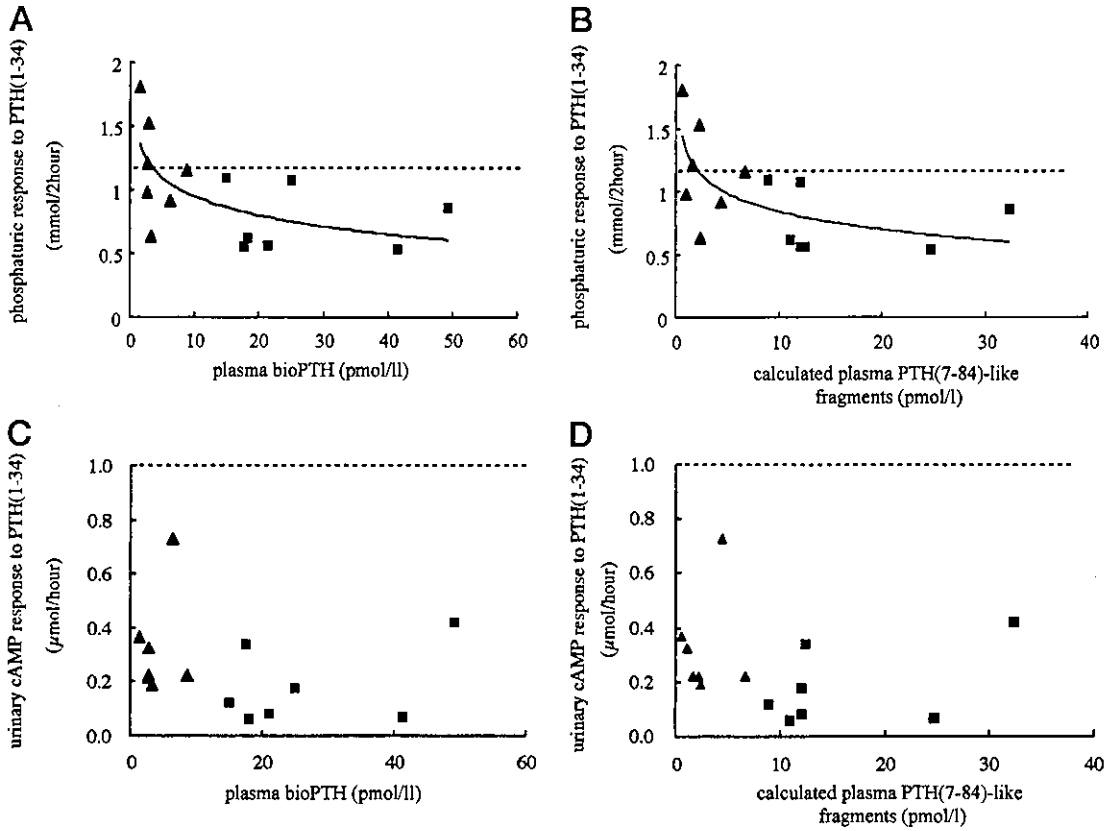

FIG. 4. The relationship between plasma PTH levels and phosphaturic response to exogenous PTH(1–34) in PHP type I patients. In the PHP patients before calcitriol treatment (■), phosphaturic responses to exogenous PTH(1–34) [the increase in urinary phosphate excretion during 2 h after infusion of 121 pmol/kg weight PTH(1–34)] were lower than 1.13 mmol/2 h, the discriminative values of phosphaturic response between PHP type I and PTH-deficient hypoparathyroidism (*dashed horizontal line*). Calcitriol treatment (1.5 μg/d) suppressed plasma levels of bioPTH and PTH(7–84)-like fragments (▲) and increased the phosphaturic response ($P < 0.05$). There was a negative correlation between plasma PTH levels and phosphaturic response. A, Phosphaturic response (mmol/2 h) = 1.93 − 0.053 × log[plasma bioPTH (pmol/liter)], r = 0.641 ($P < 0.05$). B, Phosphaturic response (mmol/2 h) = 1.78 − 0.055 × log[plasma PTH(7–84)-like fragments (pmol/liter)], r = 0.658 ($P < 0.05$). Multiplication factors to convert SI units to metric units are 8.781 for PTH(7–84)-like fragments and 3.097 for phosphate. There was not a significant difference in cAMP responses to PTH(1–34) between before and after calcitriol treatment (C and D).

only a slight increase in bioPTH. As a result, the proportion of baseline bioPTH levels to maximal bioPTH levels was 96% before calcitriol treatment (*closed circle*).

Calcitriol treatment produced complex changes in PTH-Ca dynamics and a shift of PTH-calcium curve in the horizontal direction at first and then in the vertical direction (Fig. 5). The PTH-Ca curve shifted to the right and PTH levels changed at higher calcium levels after 2 wk of calcitriol treatment (*fine dashed line*). Set point increased to 1.143 ± 0.035 mmol/liter ($P < 0.01$ *vs.* before calcitriol treatment). Then PTH-Ca curve moved downward after 25 wk of calcitriol treatment (*solid line*). Maximal bioPTH levels decreased from 255.2 ± 145.4 pg/ml (127.1 ± 0.4 pmol/liter) to 123.3 ± 36.8 pg/ml (13.1 ± 3.9 pmol/liter) ($P < 0.01$ *vs.* before calcitriol treatment). Although both baseline bioPTH levels and maximal bioPTH levels decreased after calcitriol treatment, baseline bioPTH decreased more than maximal bioPTH did. The proportion of baseline bioPTH levels to maximal bioPTH levels was 83% after 2 wk of calcitriol treatment, and the proportion decreased to 35% after 25 wk of calcitriol treatment ($P < 0.01$ *vs.* before calcitriol treatment).

Discussion

In this study, we confirmed the high circulating levels of bioPTH in PHP type I patients. We also found the high plasma levels of PTH(7–84)-like fragments and increased proportion of PTH(7–84)-like fragments to bioPTH in these patients. These results suggested the intracellular or extracellular PTH degradation as well as PTH secretion is increased in PHP type I patients. There is also the possibility the clearance of PTH(7–84)-like fragments may be decreased in these patients.

PTH(7–84) has been considered to be biologically inactive. However, Slatopolsky *et al.* (5) demonstrated antagonistic effects of PTH(7–84) on the biological activity of PTH(1–84) in rats. When PTH(1–84) and PTH(7–84) were given simultaneously, PTH(7–84) decreased the calcemic and phosphaturic responses to PTH(1–84). In the present study, phosphaturic response to exogenous PTH(1–34) was invariably impaired in PHP type I patients before calcitriol treatment when plasma levels of bioPTH and PTH(7–84)-like fragments were high. The phosphaturic response increased after

TABLE 2. Effects of calcitriol treatment on the parameters of PTH-calcium dynamics in PHP type Ib

Calcitriol treatment (wk)	0	2	25	Normal controls
Baseline Ca^{++} (mmol/liter)	0.711 ± 0.065	1.062 ± 0.049[a]	1.160 ± 0.030[a]	1.199 ± 0.044
Baseline PTH (pmol/liter)				
bioPTH	25.6 ± 13.8	21.8 ± 11.9	4.5 ± 2.6[a]	2.6 ± 0.25
iPTH	40.1 ± 22.5	34.5 ± 19.2	7.3 ± 5.3[a]	3.4 ± 0.3
PTHmax (pmol/liter)				
bioPTH	27.1 ± 15.4	26.7 ± 14.6	13.1 ± 3.9[a]	7.7 ± 1.7
iPTH	42.3 ± 23.7	39.8 ± 20.1	20.7 ± 5.0[a]	10.0 ± 2.2
Baseline PTH/PTHmax ratio				
bioPTH	0.96 ± 0.04	0.83 ± 0.08	0.35 ± 0.21[a]	0.36 ± 0.07
iPTH	0.95 ± 0.03	0.86 ± 0.10	0.36 ± 0.26[a]	0.35 ± 0.06
PTHmin (pmol/liter)				
bioPTH	5.6 ± 4.1	1.6 ± 0.9[a]	0.8 ± 0.4[a]	0.7 ± 0.3
iPTH	9.9 ± 8.3	3.2 ± 2.9[a]	1.1 ± 0.2[a]	0.9 ± 0.4
Set-point of calcium (mmol/liter)				
bioPTH	0.928 ± 0.045	1.143 ± 0.035[a]	1.129 ± 0.028[a]	1.150 ± 0.032
iPTH	0.912 ± 0.107	1.157 ± 0.038[a]	1.131 ± 0.031[a]	1.155 ± 0.035

PTH-calcium dynamics were studied by infusion of citrate and calcium in five patients with PHP type Ib and 10 normal subjects. PTHmax, Maximal PTH induced by hypocalcemia; PTHmin, minimal PTH induced by hypercalcemia; set-point of calcium, ionized calcium level at midrange between PTHmax and PTHmin. iPTH, plasma PTH levels that were measured by luminometric Nichols Advantage Intact PTH(1–84) assay, which cross-reacts with both PTH(1–84) whole molecule and PTH(7–84)-like fragments. Data are presented as means ± SD. The multiplication factor to convert Systeme Internationale units to metric units is 9.424 for PTH.

[a] $P < 0.01$ *vs.* before calcitriol treatment.

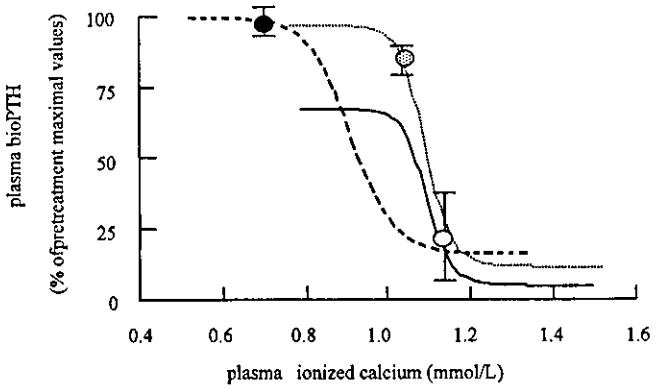

FIG. 5. PTH-calcium dynamics in PHP type Ib. BioPTH-calcium dynamics were studied by infusion of citrate and calcium in five patients with PHP type Ib before and after calcitriol treatment (1.5 μg/d). Before calcitriol treatment, bioPTH concentrations responded to the changes in calcium at low calcium levels (*coarse dashed line*). PTH-calcium curve shifted to the right after 2 wk of calcitriol treatment (*fine dashed line*) and then downward after 25 wk of treatment (*solid line*). Maximal bioPTH levels in the patients before calcitriol treatment, which was determined by citrate infusion test, were transformed to 100%. The baseline bioPTH levels were represented by circles (*closed circle*, before calcitriol treatment; *shaded circles*, after 2 wk of calcitriol treatment; *open circles*, after 25 wk of calcitriol treatment). Data are presented as means ± SD.

calcitriol treatment when plasma levels of bioPTH and PTH(7–84)-like fragments decreased. These results suggested a possibility that phosphaturic response to PTH(1–34) is modified by endogenous bioPTH and PTH(7–84)-like fragments in PHP type I patients.

In vitro study demonstrated that PTH(7–84), acting via receptors distinct from the PTH1 receptor and presumably specific for PTH-C fragments, exerts a direct antiresorptive effect on bone that may partly be due to impaired osteoclast differentiation (8). Although PHP type I is characterized by a lack of response to PTH, there is a certain preservation of bone sensitivity to PTH that was evidenced by an excessive bone remodeling (9) and normal responsiveness to PTH of bone-derived osteoblast-like cells from these patients (10). In the kidney, resistance to PTH in PHP type I patients is believed to be confined to its proximal tubular actions and does not include its distal tubular effects on Ca reabsorption (at least during treatment with 1-α hydroxylated metabolites of vitamin D) (11–13). Therefore, there is a possibility that PTH(7–84)-like fragments directly exert their biological effects or modify the action of biologically active PTH molecules on bone metabolism and renal tubular function in PHP type I patients.

In PTH-Ca dynamic studies, baseline PTH to maximum PTH ratio (B/M ratio) is thought to represent the degree of relative stimulation in baseline PTH secretion. We previously reported an inverse correlation between the B/M ratio and baseline Ca level in hypoparathyroid patients and normal subjects (7, 14). When the baseline Ca was low, the B/M ratio was high, suggesting that the parathyroids were using most of their overall capacity to correct the low Ca levels. Conversely, the increase of baseline Ca after calcitriol treatment was followed by a decrease in the B/M ratio. However, these studies were performed using a PTH assay that cross-reacts with both bioPTH and PTH(7–84)-like fragments. In the present study using a bioPTH-specific assay, we confirmed a maximally stimulated baseline PTH secretion in PHP type Ib patients. Moreover, this study demonstrated the differential inhibitory effects of calcitriol on the baseline and maximal PTH secretion. Calcitriol treatment exerted more suppressive effects on baseline secretion than maximal secretion and produced a change in relative stimulation of baseline PTH secretion in PHP type Ib.

Although acute changes in plasma Ca produced rapid responses in PTH secretion on the sigmoidal PTH-Ca curve, a sustained change in baseline plasma Ca shifts the PTH-Ca curve horizontally in the direction of the change in baseline plasma Ca. We previously reported the association between baseline plasma Ca and the set point for Ca-related PTH secretion in the hypoparathyroid patients (7, 14, 15). When

the baseline Ca levels were low before calcitriol treatment, the leftward shift of the PTH-Ca curve was observed. After calcitriol treatment, the increase in baseline Ca levels was followed by a rightward shift of the curve in the direction of the change of baseline Ca. The set point moved toward the existing plasma Ca as though parathyroid cells were capable of adapting their own specific property to the ambient plasma Ca. Such a relationship between baseline plasma Ca and the horizontal shift of the PTH-Ca curve was also observed in the present study, which was performed with bioPTH-specific assay.

In conclusion, we confirmed the increased circulating levels of PTH(1–84) whole-molecule in PHP type I patients and also found the increased PTH(7–84)-like fragments in these patients. The increased levels of these PTH molecules may be related to the impaired phosphaturic response to exogenous PTH in these patients. PTH-calcium dynamic studies revealed a maximally stimulated baseline PTH secretion in PHP type Ib. Calcitriol treatment produced a shift of sigmoidal PTH-calcium curve and a change in the degree of relative stimulation of baseline PTH secretion.

Acknowledgments

We thank Heather Pham and Dr. Kastooriranganathan Ramakrishnan (Nichols Institute Diagnostics) for technical assistance.

Received October 17, 2002. Accepted February 10, 2003.

Address all correspondence and requests for reprints to: Kazutoshi Mizunashi, M.D., Department of Internal Medicine, Senen General Hospital, Sakuragi 2-1-1, Tagajo 985-0842, Japan.

References

1. **John MR, Goodman WG, Gao P, Cantor TL, Salusky IB, Juppner H** 1999 A novel immunoradiometric assay detects full-length human PTH but not amino-terminally truncated fragments: implications for PTH measurements in renal failure. J Clin Endocrinol Metab 84:4287–4290
2. **Gao P, Scheibel S, D'Amour P, John MR, Rao SD, Schmidt-Gayk H, Cantor TL** 2001 Development of a novel immunoradiometric assay exclusively for biologically active whole parathyroid hormone 1–84: implications for improvement of accurate assessment of parathyroid function. J Bone Miner Res 16:605–614
3. **Guthrie E, Lu J, Cody C, Hutchison JS, Wong J, Carlton E, Caufield M, Nelson J, Reitz RE, Fisher DA, Segre G** 2001 Development of an automated assay that measures PTH with no crossreactivity to non-(1–84) PTH. Program of the 83rd Annual Meeting of The Endocrine Society, Denver, CO, 2001, p 473 (Abstract P3-115)
4. **Lepage R, Roy L, Brossard JH, Rousseau L, Dorais C, Lazure C, D'Amour P** 1998 A non-(1–84) circulating parathyroid hormone (PTH) fragment interferes significantly with intact PTH commercial assay measurements in uremic samples. Clin Chem 44:805–809
5. **Slatopolsky E, Finch J, Clay P, Martin D, Sicard G, Singer G, Gao P, Cantor T, Dusso A** 2000 A novel mechanism for skeletal resistance in uremia. Kidney Int 58:753–761
6. **Goto M, Mizunashi K** 2001 Decreased sensitivity of distal nephron and collecting duct to parathyroid hormone on pseudohypoparathyroidism type I. J Am Soc Nephrol 12:1965–1970
7. **Mizunashi K, Furukawa Y, Abe K, Yoshinaga K** 1993 The relationship between serum intact parathyroid hormone and calcium in idiopathic hypoparathyroidism. Calcif Tissue Int 53:378–383
8. **Divieti P, John MR, Juppner H, Bringhurst FR** 2002 Human PTH-(7–84) inhibits bone resorption *in vitro* via actions independent of the type 1 PTH/PTHrP receptor. Endocrinology 143:171–176
9. **Mizunashi K, Sohn HY, Furukawa Y** 1988 Effects of active vitamin D3 and parathyroid hormone on the serum osteocalcin in idiopathic hypoparathyroidism and pseudohypoparathyroidism. J Clin Invest 82:861–865
10. **Ish-Shalom S, Rao LG, Levine MA, Fraser D, Kooh SW, Josse RG, McBroom R, Wong MM, Murray TM** 1996 Normal parathyroid hormone responsiveness of bone-derived cells from a patient with pseudohypoparathyroidism. J Bone Miner Res 11:8–14
11. **Yamamoto M, Takuwa Y, Masuko S, Ogata E** 1988 Effects of endogenous and exogenous parathyroid hormone on tubular reabsorption of calcium in pseudohypoparathyroidism. Clin Endocrinol Metab 66:618–625
12. **Mizunashi K, Sohn HY, Furukawa Y** 1990 Heterogeneity of pseudohypoparathyroidism type I from the aspect of urinary excretion of calcium and serum levels of parathyroid hormone. Calcif Tissue Int 46:227–232
13. **Mizunashi K, Furukawa Y, Taguchi K, Kuwahara M** 1989 Effects of parathyroid hormone on urinary excretion of N-acetyl-β-D-glucosaminidase in idiopathic hypoparathyroidism and pseudohypoparathyroidism. Calcif Tissue Int 45:375–377
14. **Mizunashi K, Furukawa Y, Abe K, Takaya K, Yoshinaga K** 1995 Resetting of parathyroid hormone secretion after vitamin D_3 treatment in hypoparathyroidism and after parathyroid adenectomy in primary hyperparathyroidism. Calcif Tissue Int 57:30–34
15. **Mizunashi K, Furukawa Y, Goto MM, Abe K** 1998 Sigmoidal curve shift in idiopathic hypoparathyroidism and pseudohypoparathyroidism. Calcif Tissue Int 62:290–294

Journal of Cellular Biochemistry 93:418–426 (2004)

Involvement of Phosphoinositide 3-Kinase Signaling Pathway in Chondrocytic Differentiation of ATDC5 Cells: Application of a Gene-Trap Mutagenesis

Miyuki Ihara-Watanabe,[1] Takayuki Uchihashi,[1,2] Yoshiteru Miyauchi,[1,3] Norio Sakai,[3] Masayo Yamagata,[1,3] Keiichi Ozono,[3] and Toshimi Michigami[1,2]*

[1]Department of Environmental Medicine, Osaka Medical Center and Research Institute for Maternal and Child Health, Izumi, Osaka 594-1101, Japan
[2]Department of Craniofacial Developmental Biology, Osaka University Graduate School of Dentistry, Suita, Osaka 565-0871, Japan
[3]Department of Pediatrics, Osaka University Graduate School of Medicine, Suita, Osaka 565-0871, Japan

Abstract Gene-trap mutagenesis is based on the notion that the random insertion of a trapping vector may disturb the function of inserted genes. Here, we applied this method to murine mesenchymal ATDC5 cells, which differentiate into mature chondrocytes in the presence of insulin. As the trap vector we used pPT1-geo, which lacks its own promoter and enhancer, but contains a *lacZ–neo* fusion gene as a reporter and selection marker driven by the promoter of the trapped gene. After pPT1-geo was introduced into ATDC5 cells by electroporation, the neomycin-resistant clones were screened for β-galactosidase activity. The selected clones were cultured in differentiation medium to evaluate the chondrogenic phenotype. The clones no. 6–30 and 6–175, which exhibited impaired and accelerated mineralization, respectively, were subjected to further analysis. In clone no. 6–30 in which the gene coding for the p85α subunit of phosphoinositide 3-kinase (PI3K) was trapped, the expression of marker genes of early chondrocytes including collagen type II, aggrecan, and PTH/PTHrP receptor was delayed. The insulin-induced stimulation of growth was reduced in clone no. 6–30 compared with the parental ATDC5 cells. Moreover, treatment of parental ATDC5 cells with a specific inhibitor of PI3K, LY294002, phenocopied clone no. 6–30, suggesting the involvement of PI3K signaling in the chondrogenic differentiation of ATDC5 cells. Clone no. 6–175 with accelerated mineralization was revealed to have a gene homologous to human KIAA0312 trapped, whose function remains unclear. Taken together, the gene-trap in ATDC5 cells might be useful to identify the molecules involved in chondrogenic differentiation. J. Cell. Biochem. 93: 418–426, 2004.

Key words: gene-trap; chondrocyte; ATDC5; phosphoinositide 3-kinase; insulin

Endochondral bone formation is a multistep phenomenon consisting of mesenchymal condensation of undifferentiated cells, proliferation of chondrocytes, and differentiation into hypertrophic chondrocytes, followed by mineralization [de Crombrugghe et al., 2001]. During maturation, chondrocytes change morphologically, and exhibit alterations in the production of extracellular matrix proteins. Hypertrophic chondrocytes are characterized by a high level of alkaline phosphatase (ALP), diminished levels of collagens type II and IX, and the production of type X collagen, a hypertrophic chondrocyte-specific product. Various kinds of signaling molecules, including Indian hedgehog, parathyroid hormone-related protein (PTHrP), and fibroblast growth factors (FGFs)

Grant sponsor: Ministry of Education, Science and Culture of Japan (grants-in-aid for scientific research to TM and KO); Grant sponsor: Novo Nordisk Pharma. Ltd. (Fund to KO); Grant sponsor: Ministry of Education, Culture, Sports, Science and Technology of Japan (to TM for the 21st century COE entitled "Origination of Frontier Bio-Dentistry" at "Osaka University Graduate School of Dentistry").

*Correspondence to: Toshimi Michigami, MD, PhD, Department of Environmental Medicine, Osaka Medical Center and Research Institute for Maternal and Child Health, 840 Murodo-cho, Izumi, Osaka 594-1101, Japan.
E-mail: michigami@lab.mch.pref.osaka.jp

Received 6 February 2004; Accepted 4 May 2004
DOI 10.1002/jcb.20185
Published online 20 July 2004 in Wiley InterScience (www.interscience.wiley.com).

have been revealed to regulate the maturation of chondrocytes [Karaplis et al., 1994; Lanske et al., 1996; Vortkamp et al., 1996; St-Jacques et al., 1999; Liu et al., 2002; Minina et al., 2002; Ohbayashi et al., 2002]. However, the molecular mechanisms underlying the proliferation and differentiation of chondrocytes are still not fully understood.

Gene-trapping is a genome-wide approach applied to clarify the functions of genes by random insertion of a trapping vector which might disturb the function of the inserted genes [Stanford et al., 1998; Stanford et al., 2001]. In essence, a gene-trap vector consists of a promoterless reporter gene, a selectable marker and a splice acceptor site immediately upstream of the reporter gene [Stanford et al., 2001]. When the gene-trap vector is appropriately inserted in the endogenous gene, a fusion transcript including the upstream coding sequence of the gene and the reporter gene is generated by the endogenous *cis*-acting promoter and enhancer element of the trapped gene. This event is associated with the conversion of the trapped gene into a mutated gene and allows one to examine its expression pattern by visualization of the reporter activity. This approach is usually applied in embryonic stem (ES) cells to analyze the effect of gene trapping in individuals such as gene-trapped mice. At present, several large-scale, gene-trap screens are being carried out with various vectors, which aim to generate a public resource of mutagenized ES cells [Stanford et al., 2001].

The clonal cell line, ATDC5, is a commonly used cell model of endochondral ossification [Akiyama et al., 1996; Syukunami et al., 1996; Syukunami et al., 1997]. ATDC5 was originally isolated from the murine feeder-independent teratocarcinoma stem cell line AT805 on the basis of chondrogenic potential [Atsumi et al., 1990]. In the presence of insulin, the confluent monolayer culture of ATDC5 cells differentiate into proliferating chondrocytes through a cellular condensation process and undergo cellular hypertrophy and mineralization in the absence of β-glycerophosphate [Syukunami et al., 1997]. In other words, ATDC5 cells reproduce the multistep chondrocytic differentiation process encompassing the stages from mesenchymal condensation to calcification in vitro, which enables the study of the molecular mechanisms underlying endochondral bone formation.

In the present study, to identify the genes involved in chondrocytic differentiation, we applied a gene-trap approach in ATDC5 cells. One of the trap clones, which exhibited impaired mineralization, was identified to have trapped the gene encoding the p85α subunit of phosphatidylinositide 3-kinase (PI3K). Here, we demonstrate the usefulness of gene-trap mutagenesis in ATDC5 cells for investigating the molecular mechanisms of chondrocytic differentiation.

MATERIALS AND METHODS

Cell Culture

For chondrogenic induction, parental ATDC5 cells or the trap clones were inoculated into six-well culture plates (5×10^5 cells/well) and cultured in a 1:1 mixture of Dulbecco's modified Eagle's and Ham's F12 (DMEM/F12) medium containing 5% fetal bovine serum (FBS: ICN Biomedicals, Aurora, OH), insulin–transferrin–selenium-G supplement (ITS: Invitrogen, Carlsbad, CA; insulin 10 μg/ml, sodium selenite 6.7 μg/ml, and transferrin 5.5 mg/ml as a final concentration) at 37°C in a 5% CO2 atmosphere. After 3 days later, the medium was changed to alpha minimal essential medium (αMEM) supplemented with 5% FBS and ITS, and the culture plates were sealed with adhesive tape to facilitate mineralization. The medium was replaced every 3 days.

To evaluate the proliferation, parental ATDC5 cells, or the trap clones were inoculated into six-well culture plates at a density of 1×10^4/well, and cultured in DMEM/F12 containing 5% FBS in the presence or absence of insulin (10 μg/ml; Sigma, St. Louis, MO). The cell number in each well was then sequentially determined after trypsinization. In some experiments, the effects of specific PI3K inhibitor LY294002 (Sigma) were examined.

Gene-Trapping

As the trap vector, we used pPT1-geo, which lacks its own promoter and enhancer, but contains an *Escherichia coli* (*E. coli*) *lacZ* gene encoding β-galactosidase as a reporter fused to an *E. coli* neomycin resistance gene as a selection marker, which was designated *lacZ–neo* [Mainguy et al., 2000; Fig. 1]. The fusion gene *lacZ–neo* is assumed to be driven by the promoter of the trapped gene. Since the trap vector contains a splice acceptor site from the murine engrailed-2 gene upstream of *lacZ–neo*,

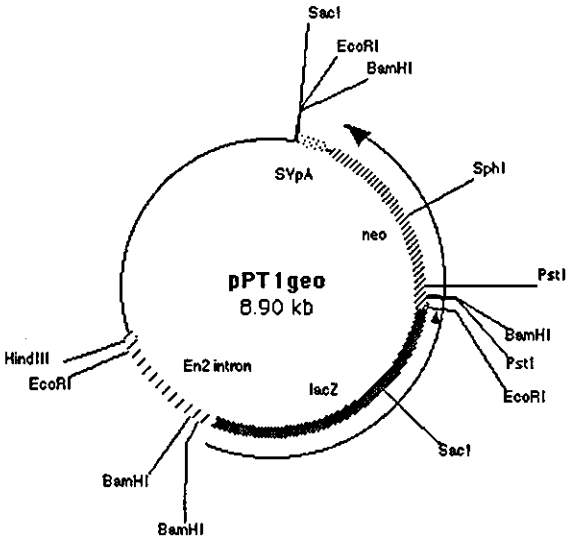

Fig. 1. Structure of the trapping vector pPT1-geo. It lacks its own promoter and enhancer, but contains a *lacZ–neo* fusion gene as a reporter and a selection marker driven by the promoter of the trapped gene.

its integration in the intron leads to a fusion transcript being generated from the upstream exon of the trapped gene, the exon of engrailed-2 and *lacZ–neo* on transcriptional activation of the trapped gene. After pPT1-geo linearized with *Hind*III digestion was introduced into ATDC5 cells using the Gene Pulser II electroporation system (BioRad, Helcules, CA), the neomycin-resistant clones were selected in the presence of G418 (400 μg/ml, Invitrogen). Then the neomycin-resistant clones (815 clones in total) were screened for β-galactosidase activity. Among them, 26 clones with a 100-fold higher level of β-galactosidase activity than the parental ATDC5 cells were then subjected to chondrogenic induction, followed by alcian blue and alizarin red staining to evaluate the extracellular matrix production and mineralization, respectively.

Identification of the Trapped Genes by 5′-Rapid Amplification of cDNA End (RACE)

Total RNA was extracted from trap clones using TRIZOL reagent (Invitrogen), and messenger RNA purified with oligo(dT) latex (Oligotex™-dT30 Super mRNA Purification Kit; Takara Biomedicals, Shiga, Japan). To identify the trapped genes, 5′-RACE was performed utilizing the 5′-RACE System for RACEs (Invitrogen), according to the manufacturer's instructions with some modifications. Briefly, first-strand cDNA was synthesized from mRNA (1 μg) using SuperScript II reverse transcriptase (Invitrogen) with a primer specific to *lacZ* cDNA in pPT1-geo; LacZ-GSP1, 5′-TGGCGAAAGGGGGATGTG-3′. After the first strand of cDNA was synthesized, the original mRNA template was removed by treatment with RNase, and the unincorporated dNTPs and the primer were separated from the cDNA using a GlassMAX Spin Cartridge (Invitrogen). Then a homopolymeric tail was added to the 3′-end of the cDNA using TdT and dCTP, followed by PCR amplification using Taq polymerase (Promega, Madison, WI) and the following set of primers; 5′RACE Abridged Anchor Primer, 5′-GGCCACGCGTCGACTAGTACGGGIIGGGIIGGGIIG-3′ (I; inosine) and LacZ-GSP2, 5′-ATGTGCTGCAAGGCGATTAAGTTG-3′. The PCR product then served as the template for the second round of PCR using the primers LacZ-GSP3, 5′-CCAGGGTTTTCCCAGTC-3′, and 5′RACE-AUAP, 5′-GGCCACGCGTCGACTAGTAC-3′. The product of the second PCR was then cloned into pT7-Blue vector (Novagen, Madison, WI) and sequenced using an automated sequencer (377A model; PE Applied Biosystems, Tokyo, Japan).

Reverse Transcription-Polymerase Chain Reaction (RT-PCR)

Total RNA (2.5 μg) prepared as above was reverse transcribed using random hexamer (Promega) and SuperScript II (Invitrogen). PCR was performed using Taq polymerase (Promega) and murine-specific primer sets as follows; murine type II collagen pro α1 chain, sense, 5′-TCTCCACTCTTCTAGTTCCT-3′ and antisense, 5′-TTGGGTCATTTCCACATGC-3′; murine aggrecan, sense, 5′-ACTATGACCACTTTACTCTTGG-3′ and antisense, 5′-TGGCGATGATGGCGCTGTTCTG-3′; PTH/PTHrP receptor sense, 5′-ATGCTCTTCAACTCCTTCCAG-3′ and antisense, 5′-ACTGGCTTCTTGGTCCATCTG-3′; GAPDH sense, 5′-CCCATCACCATCTTCCAGGA-3′ and antisense, 5′-TTGTCATACCAGGAAATGAGC-3′. Amplification of the expected fragments was confirmed by sequencing of the products.

Measurement of ALP Activity

ALP activity was measured by the Lowry method using *p*-nitrophenylphosphate as a substrate in an alkaline glycine buffer containing 10 mM $MgCl_2$ and standardized to the protein amount [Lowry et al., 1954].

Western Blotting

Whole cell extracts were harvested in RIPA buffer [1% Triton, 1% Na deoxycholate, 0.1% SDS, 150 mM NaCl, 10 mM Tris-Cl (pH 7.4), 5 mM EDTA, and protease inhibitor cocktail (Complete^{TM}; Roche Diagnostics GmbH, Mannheim, Germany)]. The cell lysates containing 10 μg of each protein were then subjected to SDS–PAGE, and were transferred to PVDF membrane (Biorad). After blocking with Block Ace reagent (Dainippon Pharmaceuticals, Osaka, Japan), the membranes were incubated with the following primary antibodies; anti-PI3K p85α monoclonal antibody (B-9, Santa Cruz Biotechnology, Santa Cruz, CA), or anti-β galactosidase polyclonal antibody (Rockland, Gilbertsville, PA). After incubation with the corresponding secondary antibodies, the proteins were visualized using the enhanced chemiluminescence detection system (Amersham Biosciences, Piscataway, NJ).

Southern Blot Analysis

Genomic DNA was extracted from parental ATDC5 cells and trap clones, and digested with the enzymes *Sph*I or *Pst*I. The digested DNA was then electrophoresed, transferred to a Hybond-N+ membrane (Amersham Biosciences), and probed with a radiolabeled fragment of *lacZ* cDNA prepared by *Eco*RI / *Sac*I digestion of pPT1-geo.

RESULTS

Isolation of A Clone With the Gene Encoding the PI3K p85α Subunit Trapped

As described in "Materials and Methods," we obtained 815 neomycin-resistant clones. Since trap vector pPT1-geo possesses the *lacZ–neo* fusion gene which should be driven under the control of the trapped gene promoter, the trapped clones can be isolated under the selection with neomycin only when the trapped genes are expressed in ATDC5 cells. Among them, 26 clones with strong β-galactosidase activity were subjected to chondrogenic induction in the presence of insulin. We performed alcian blue and alizarin red staining of these cells at 5 and 7 weeks of culture, respectively. In alizarin red staining, 8 clones exhibited accelerated mineralization, while 14 clones showed delayed mineralization compared with the parental ATDC5 cells (data not shown). One of

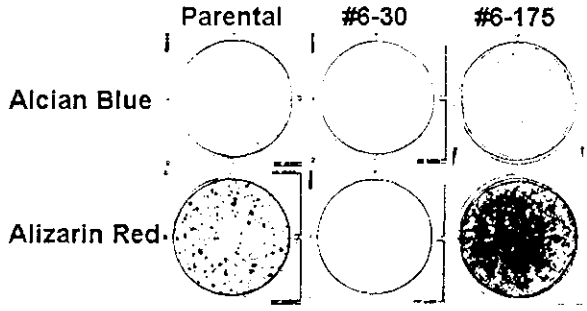

Fig. 2. Alcian blue and alizarin red staining of parental ATDC5 cells and the trap clones no. 6–30 and 6–175 cultured in the presence of insulin. The cells were inoculated into six-well culture plates (5×10^5 cells/well) and cultured in DMEM/F12 medium containing 5% FBS and 10 μg/ml of insulin at 37 C in a 5% CO_2 atmosphere. After 3 days, the medium was changed to αMEM containing 5% FBS and 10 μg/ml of insulin, and the culture plates were sealed with adhesive tape to facilitate the mineralization. The medium was replaced every 3 days. Alcian blue and alizarin red staining were performed on day 35 and day 49, respectively.

the clones, no. 6–30, accumulated less of a cartilageous matrix than the parental ATDC5 cells as shown by alcian blue staining (Fig. 2). In addition, alizarin red, which stains mineralized matrices, revealed reduced mineralization in this clone (Fig. 2). 5′-RACE analysis showed that the trapping vector was inserted in intron 1 of the gene encoding the p85α subunit of PI3K in the clone no. 6–30. On the other hand, the clone no. 6–175 with accelerated mineralization (Fig. 2) was revealed to have a gene homologous to human KIAA0312 trapped, whose function remains unclear. Since we obtained both clones with delayed mineralization and accelerated mineralization, we assume that trapping of the genes was responsible for the phenotypical change of these clones. In the clone no. 6–30, the trapped allele was assumed to express a fusion protein containing the N-terminal Src homology 3 (SH3) region of the p85α subunit transcribed from exon 1A and the product of the *lacZ–neo* fusion gene, but lacking the SH2 domains and the domain responsible for interaction with p110 (Fig. 3). Western blot analysis using monoclonal antibody against p85α which recognizes amino acids 333–430 mapping within the amino terminal SH2 domain, demonstrated the reduced expression of p85α in the trap clone no. 6–30, since the fusion protein from the trapped allele was not recognized by the antibody (Fig. 4, left panel). Because one of the p85α alleles remained intact, residual expression of the protein was detected in the

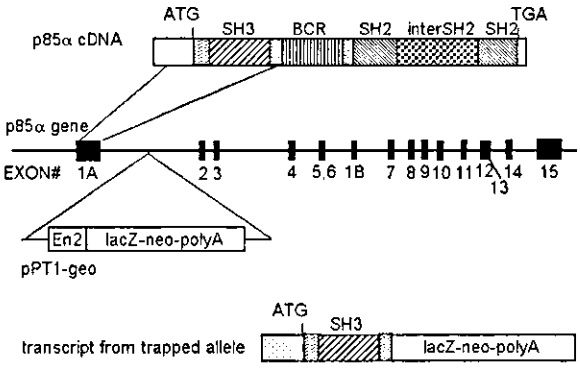

Fig. 3. Schematic representation of the genomic organization of the murine *p85α* gene and the insertional mutation resulting from gene-trapping with the vector pPT1-geo. The locations of exons (solid boxes) and introns (horizontal lines between exons) are indicated. SH3; Src homology 3 domain, BCR; the breakpoint cluster region homology domain, SH2; Src homology 2 domain. En2; murine engrailed-2 exon, lacZ–neo–polyA; fusion gene of *lacZ–neo*. ATG indicates an initiation codon, and TGA is the termination codon.

clone. When the antibody against β-galactosidase was utilized as the primary antibody, only one band was detected corresponding to the fusion of part of p85α and the *lacZ*-neo product, indicating that only one fusion gene was expressed (Fig. 4, right panel, arrowhead). Although Southern blot analysis using *lacZ* cDNA as the probe suggested that the trap vector had been

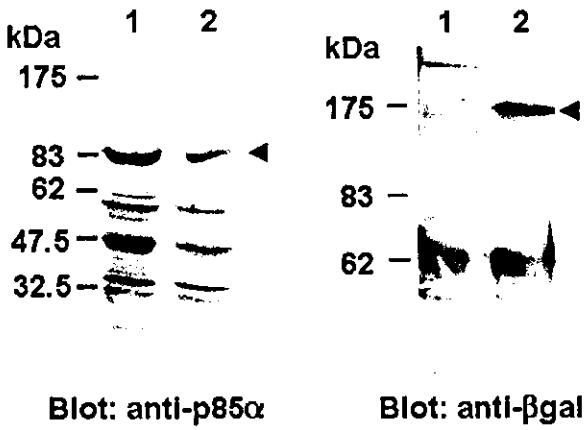

Fig. 4. Detection of the p85α subunit by Western blot analysis. Whole cell lysates obtained from the parental ATDC5 cells (**lane 1**) and the trap clone no. 6–30 (**lane 2**) were subjected to SDS–PAGE, followed by immunoblotting using antibody against amino acids 333–430 mapping within the SH2 domain of p85α (**left panel**) or antibody against β-galactosidase (**right panel**). The arrowhead in the left panel shows the signal corresponding to the wild-type protein of p85α. On the other hand, the arrowhead in the right panel indicates the signal corresponding to the fusion protein of part of p85α and the lacZ–neo product.

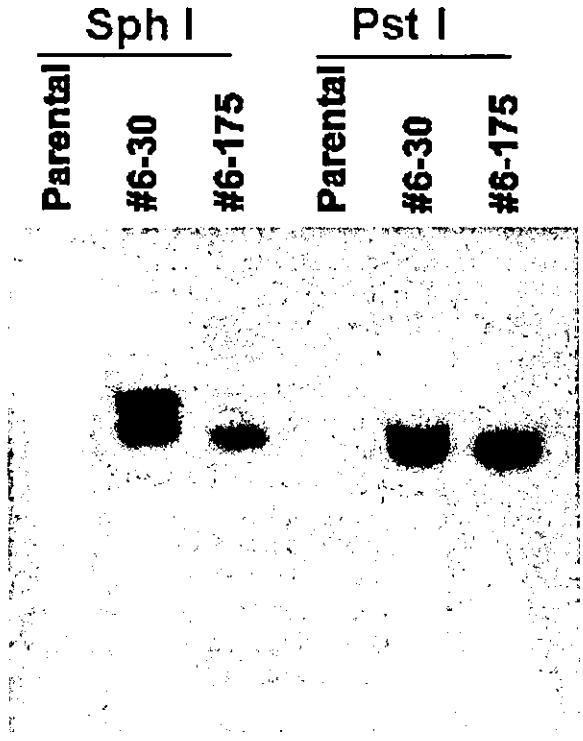

Fig. 5. Southern blot analysis. Genomic DNA extracted from the parental ATDC5 cells or the trap clones no. 6–30 and 6–175 was digested with the restriction enzymes SphI or PstI, and subjected to Southern blot analysis using a radiolabeled fragment of lacZ cDNA prepared by *Eco*RI/*Sac*I digestion of pPT1-geo as the probe.

inserted into two locations in the genome of the clone no. 6–30 (Fig. 5) and FISH analyses confirmed it (data not shown), only one product was amplified by 5′-RACE, suggesting that an insertion other than that into the *p85α* gene was likely to occur in non-coding DNA or a gene that was not expressed in ATDC5 cells. As to the clone no. 6–175, integration of the trap vector into a single location was detected in the Southern analysis (Fig. 5).

Impairment of the Insulin-Induced Stimulation of Proliferation in no. 6–30

Parental ATDC5 cells and the trap clone no. 6–30 were cultured in the presence or absence of 10 μg/ml of insulin, and the proliferation of these cells was evaluated. In the absence of insulin, there was no significant difference in growth between parental ATDC5 cells and the trap clone no. 6–30 (Fig. 6). In the presence of insulin, the growth was accelerated both in parental ATDC5 cells and in no. 6–30. However, the insulin-induced stimulation of proliferation

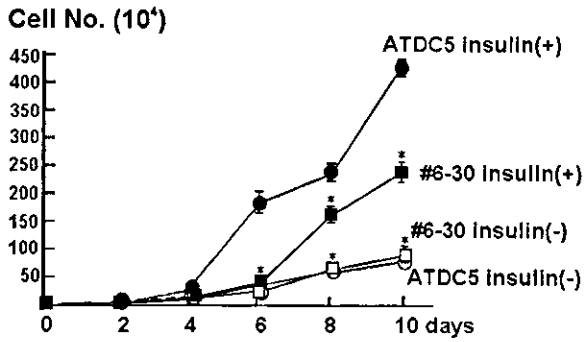

Fig. 6. Growth curves of the parental ATDC5 cells and the clone no. 6-30 cultured in the presence (closed circle; parental ATDC5, closed rectangle; no. 6-30) or absence (open circle; parental ATDC5, open rectangle; no. 6-30) of 10 μg/ml of insulin. The data are expressed as mean ± SE (n = 3). *Significantly different from the values in the insulin-treated parental ATDC5 cells ($P < 0.001$). The experiments were performed three times with similar results.

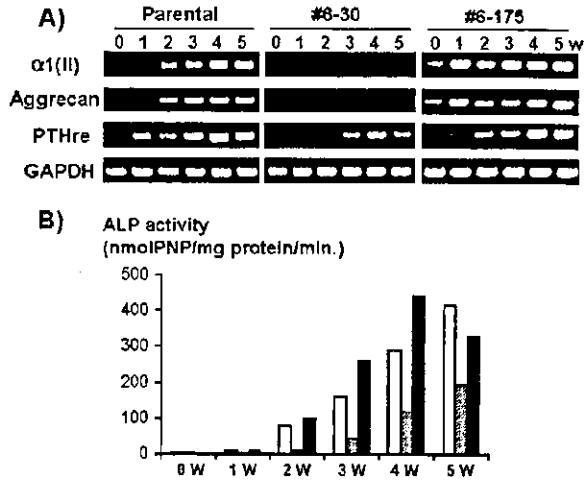

Fig. 7. A: RT-PCR analysis for the expression of marker genes of early chondrocytes. Total RNA was extracted from the parental ATDC5 cells or the trap clones no. 6-30 and 6-175 cultured in the presence of insulin (10 μg/ml) for the period indicated, and was subjected to RT-PCR analysis for the expression of type II collagen proα1 chain [α1(II)], aggrecan, PTH/PTHrP receptor (PTHre), and GAPDH. B: ALP activity in the parental ATDC5 cells (open columns), the trap clones no. 6-30 (hatched columns), and no. 6-175 (closed columns). Cell lysates were harvested from the cells cultured in the presence of insulin for the period indicated, and subjected to measurement of ALP activity. The experiments were repeated three times, and similar results were obtained.

was markedly reduced in no. 6-30 compared to the parental cells (Fig. 6).

Impaired Differentiation in the Trap Clone no. 6-30

The chondrogenic phenotype of no. 6-30 was analyzed by RT-PCR. The expression of collagen type II, aggrecan, and PTH/PTHrP receptor, which are the markers of early chondrogenesis, were suppressed in the trap clone compared with the parental cells (Fig. 7A). In addition, ALP activity was reduced in no. 6-30 compared with the parental cells or trap clone no. 6-175 (Fig. 7B).

Treatment of Parental ATDC5 Cells With PI3K Inhibitor LY294002 Mimicked the Phenotype of the Trap Clone no. 6-30

Treatment of parental ATDC5 cells with the specific inhibitor of PI3K LY294002 (10 μM) markedly inhibited insulin-induced stimulation of proliferation of the parental ATDC5 cells (Fig. 8A). In addition, treatment of parental ATDC5 cells with LY294002 (10 μM) suppressed the accumulation of cartilageous matrix and the mineralization as shown by alcian blue and alizarin red staining, respectively (Fig. 8B).

DISCUSSION

Here, we utilized a gene-trap approach to identify the genes involved in chondrocytic differentiation. Gene-trap mutagenesis is a technique that randomly generates loss-of-function mutations and reports the expression of many mouse genes [Stanford et al., 1998; Stanford et al., 2001]. Although this approach is usually carried out using ES cells to generate and analyze mutant mice derived from mutagenized

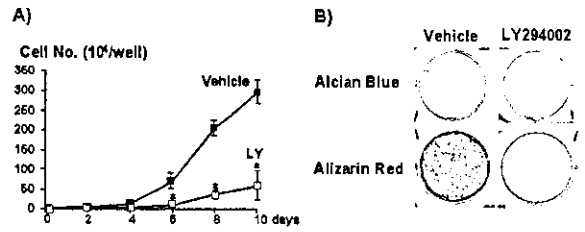

Fig. 8. A: Effect of LY294002 on the proliferation of parental ATDC5 cells. ATDC5 cells were cultured with 10 μM of LY294002 (open rectangles) or vehicle (closed rectangles) in the presence of 10 μg/ml of insulin, and the cell number was determined after the indicated culture period. The data are expressed as mean ± SE (n = 3). *Significantly different from the values in the vehicle-treated cells ($P < 0.001$). The experiments were performed three times with similar results. B: Effect of LY294002 on matrix accumulation and mineralization of parental ATDC5 cells. ATDC5 cells were cultured with 10 μM of LY294002 or vehicle in αMEM containing 5% FBS and 10 μg/ml of insulin. Alcian blue and alizarin red staining were performed on day 35 and 49, respectively.

ES cell lines, here we applied the strategy to ATDC5 cells that can differentiate into mature chondrocytes in vitro. One of the advantages of gene-trapping in ATDC5 cells is assumed to be that it does not require the large amount of space that is indispensable to screen gene-trapped mice. In addition, ATDC5 cells differentiate into mature hypertrophic chondrocytes with a mineralized matrix in several weeks when cultured in the presence of insulin, which enables one to screen the trap clones by phenotype in a relatively short time. On the other hand, gene-trapping in ATDC5 cells also has limitations: because the wild-type alleles remain, the clones in which some recessive genes are trapped will be missed in the screening by phenotype. However, in cases where the trapped genes have a dose effect or the trapping results in a fusion protein with a dominant-negative effect, one can expect the clones to exhibit a unique phenotype in terms of chondrocytic differentiation.

In the current study, among the clones screened, one with impaired mineralization was revealed to have the gene encoding the p85α subunit of PI3K trapped. In this particular clone, Southern blot analysis revealed that the trap vector was inserted at two locations in the genome (Fig. 5). However, since the only one product was amplified by 5′ RACE, an insertion other than that in the *p85α* gene was likely to occur in non-coding DNA or a gene that was not expressed in ATDC5 cells. Therefore, we assume that the phenotypic change in this clone resulted from the trapping of the *p85α* gene. In addition, treatment of parental ATDC5 cells with the PI3K inhibitor LY294002 mimicked the phenotype of the clone with the *p85α* gene trapped (Fig. 8). These results further support that the insertion of the trapped vector in the *p85α* gene is responsible for the impairment of chondrogenic differentiation of ATDC5 cells.

PI3K, a heterodimeric enzyme consisting of a regulatory subunit such as p85α and a 110-kDa catalytic subunit (p110), has been implicated in the regulation of various cellular events, including proliferation, differentiation, and survival in response to many kinds of cytokines and growth factors. Phosphorylated tyrosine residues in receptors and non-receptor proteins such as insulin receptor substrate-1 (IRS-1) interact with the SH2 domain in the regulatory subunit of PI3K, resulting in the activation or recruitment of the enzyme [Toker and Cantley, 1997]. Among the five regulatory subunits of PI3K that have been identified to date, p85α was the first to be cloned [Fruman et al., 1996]. The p85α molecule contains two Src homology 2 (SH2) domains, an N-terminal SH3 domain, and a domain responsible for binding to p110, which is located between the two SH2 domains. The other regulatory subunits p55α and p50α are generated by alternative splicing of the *p85α* gene, and exhibit different PI3K activity-elevating responses to insulin [Pons et al., 1995; Inukai et al., 1996; Inukai et al., 1997].

In our clone with the *p85α* gene trapped, the protein amount of p85α was obviously reduced, which was confirmed by Western blotting using antibody against amino acids 333–430 mapping within the SH2 domain (Fig. 4). Consistent with this result, the insulin-induced stimulation of proliferation was reduced in the trap clone compared with the parental ATDC5 cells (Fig. 6). The decreased response to insulin leads to impaired mesenchymal condensation and impaired expression of the marker genes for early chondrocytes in the trap clone no. 6–30. Moreover, treatment of parental ATDC5 cells with specific inhibitor of PI3K, LY294002, mimicked the phenotype of the trap clone 6–30; suppressed the insulin-induced stimulation of proliferation and impaired the mineralization (Fig. 8). These results indicated the involvement of PI3K in the early stages of the chondrocytic differentiation of ATDC5 cells. In vivo, IGF-I might be the major signal instead of insulin which acts through PI3K in the process of chondrogenesis.

To date, several mouse lines have been generated that lack the product of the *p85α* gene by gene targeting [Fruman et al., 1999; Suzuki et al., 1999; Terauchi et al., 1999]. No phenotypic changes in the skeleton have been reported in these animals. However, the involvement of the PI3K/Akt pathway in bone metabolism has been suggested by a line of in vitro studies [Borgatti et al., 2000; Ghosh-Choudhury et al., 2002; Peng et al., 2003]. Borgatti et al. [2000] reported that exposure to proliferative growth factors induced the nuclear translocation of Akt in osteoblastic MC3T3-E1 cells. It has also been reported that the PI3K/Akt signaling pathway is involved in bone morphogenetic protein-2 (BMP-2)-induced osteoblastic differentiation [Ghosh-Choudhury et al., 2002]. In addition, Peng et al. [2003] have recently reported that mice lacking both Akt1 and Akt2 exhibit

delayed bone development as well as impaired skin development, skeletal muscle atrophy, and impeded adipogenesis. Our findings using the clone where the *p85α* gene was trapped may enhance the importance of the PI3K pathway in mesenchymal cell proliferation and differentiation in response to extracellular stimuli.

In this study, we have also isolated the clone no. 6–175 which exhibited accelerated mineralization (Fig. 2). 5'RACE revealed that a gene homologous to human KIAA0312 has been trapped in this clone. Although the functions of this molecule are still unclear, it contains a HECT domain-like motif characteristic to a subtype of ubiquitin E3 ligase. Whether this molecule really acts as an E3 ligase remains to be elucidated.

In conclusion, a gene-trap approach revealed that PI3K plays some roles in the early steps of chondrocytic differentiation in ATDC5 cells. Although there are some limitations to gene trapping in ATDC5 cells, it is a useful strategy for identifying molecules that might be involved in chondrocytic differentiation.

ACKNOWLEDGMENTS

We thank Dr. Wolfgang Wurst and Dr. Mika Karasawa (the German Gene Trap Consortium) for providing us the trap vector pPT1-geo. We also thank Dr. Youichi Matsuda (Trans Animex, Co., Ltd.) for performing FISH analysis and Ms. Tomoko Hayashi for her secretarial help. This work was a part of the 21st Century COE entitled "Origination of Frontier BioDentistry" at "Osaka University Graduate School of Dentistry" supported by the Ministry of Education, Culture, Sports, Science and Technology of Japan.

REFERENCES

Akiyama H, Hiraki Y, Shigeno C, Kohno H, Syukunami C, Tsuboyama T, Kasai R, Suzuki F, Konishi J, Nakamura T. 1996. 1α, 25-dihydroxyvitamin D_3 inhibits cell growth and chondrogenesis of a clonal mouse EC cell line, ATDC5. J Bone Miner Res 11:22–28.

Atsumi T, Miwa Y, Kimata K, Ikawa Y. 1990. A chondrogenic cell line derived from a differentiating culture of AT805 teratocarcinoma cells. Cell Diff Dev 30:109–116.

Borgatti P, Martelli AM, Bellacosa A, Casto R, Massari L, Capitani S, Neri LM. 2000. Translocation of Akt/PKB to the nucleus of osteoblast-like MC3T3-E1 cells exposed to proliferative growth factors. FEBS Lett 477:27–32.

de Crombrugghe B, Lefebvre V, Nakashima K. 2001. Regulatory mechanisms in the pathways of cartilage and bone formation. Curr Opin Cell Biol 13:721–727.

Fruman DA, Cantley LC, Carpenter CL. 1996. Structural organization and alternative splicing of the murine phosphoinositide 3-kinase *p85α* gene. Genomics 37: 113–121.

Fruman DA, Snapper SB, Yballe CM, Davidson L, Yu JY, Alt FW, Cantley LC. 1999. Impaired B cell development and proliferation in absence of phosphoinositide 3-kinase *p85α*. Science 283:393–397.

Ghosh-Choudhury N, Abboud SL, Nishimura R, Celeste A, Mahimainathan L, Ghosh Chondhury G. 2002. Requirement of BMP-2-induced phosphatidylinositol 3-kinase and Akt serine/threonine kinase in osteoblast diffentiation and Smad-dependent BMP-2 gene transcription. J Biol Chem 277:33361–33368.

Inukai K, Anai M, Breda EV, Hosaka T, Katagiri H, Funaki M, Fukushima Y, Ogihara T, Yazaki Y, Kikuchi M, Oka Y, Asano T. 1996. A novel 55-kDa regulatory subunit for phosphatidylinositol 3-kinase structurally similar to p55PIK is generated by alternative splicing of the *p85α* gene. J Biol Chem 271:5317–5320.

Inukai K, Funaki M, Ogihara T, Katagiri H, Kanda A, Anai M, Fukushima Y, Hosaka T, Suzuki M, Shin B-C, Takata K, Yazaki Y, Kikuchi M, Oka Y, Asano T. 1997. *p85α* gene generates three isoforms of regulatory subunit for phosphatidylinositol 3-kinase (PI3-kinase), p50α, p55α, and p85α, with different PI3-kinase activity elevating responses to insulin. J Biol Chem 272:7873–7882.

Karaplis AC, Luz A, Glowacki J, Bronson RT, Tybulewics VL, Kronenberg HM, Mulligan RC. 1994. Lethal skeletal dysplasia from targeted disruption of the parathyroid hormone-related peptide gene. Genes Dev 8:277–289.

Lanske B, Karaplis AC, Lee K, Luz A, Vortkamp A, Pirro A, Karperien M, Defize LH, Ho C, Mulligan RC, et al. 1996. PTH/PTHrP receptor in early development and Indian hedgehog-regulated bone growth. Science 273:663–666.

Liu Z, Xu J, Colvin JS, Ornitz DM. 2002. Coordination of chondrogenesis and osteogenesis by fibroblast growth factor 18. Genes Dev 16:859–869.

Lowry OH, Roberts NR, Wu ML, Hixon WS, Crawford EJ. 1954. The quantitative histochemistry of brain. II. Enzyme Measurements. J Biol Chem 207:19–37.

Mainguy G, Montesinos ML, Lesaffre B, Zevnik B, Karasawa M, Kothary R, Wurst W, Prochiantz A, Volovitch M. 2000. An induction gene trap for identifying a homeoprotein-regulated locus. Nat Biotechnol 18:746–749.

Minina E, Kreschel C, Naski MC, Ornitz DM, Vortkamp A. 2002. Interaction of FGF, Ihh/PthIh, and BMP signaling integrates chondrocyte proliferation and hypertrophic differentiation. Dev Cell 3:439–449.

Ohbayashi N, Shibayama M, Kurotaki Y, Imanishi M, Fujimori T, Itoh N, Takada S. 2002. FGF18 is required for normal cell proliferation and differentiation during osteogenesis and chondrogenesis. Genes Dev 16:870–879.

Peng XD, Xu PZ, Chen ML, Hahn-Windgassen A, Skeen J, Jacobs J, Sundararajan D, Chen WS, Crawford SE, Colemen KG, Hay N. 2003. Dwarfism, impaired skin development, skeletal muscle atrophy, delayed bone development, and impeded adipogenesis in mice lacking Akt1 and Akt2. Gene Dev 17:1352–1365.

Pons S, Asano T, Glasheen E, Miralpeix M, Zhank Y, Fisher TL, Myers MG, Jr., Sun XJ, White MF. 1995. The structure and function of $p55^{PIK}$ reveal a new regulatory

subunit for phosphatidylinositol 3-kinase. Mol Cell Biol 15:4453–4465.

St-Jacques B, Hammerschmidt M, McMahon AP. 1999. Indian hedgehog signaling regulates proliferation and differentiation of chondrocytes and is essential for bone formation. Genes Dev 13:2072–2086.

Stanford WL, Caruana G, Vallis KA, Inamdar M, Hidaka M, Bautch VL, Bernstein A. 1998. Expression trapping: Identification of novel genes expressed in hematopoietic and endothelial lineages by gene trapping in ES cells. Blood 92:4622–4631.

Stanford WL, Cohn JB, Cordes SP. 2001. Gene-trap mutagenesis: Past, present, and beyond. Nat Rev Genet 2:756–768.

Suzuki H, Terauchi Y, Fujiwara M, Aizawa S, Yazaki Y, Kadowaki T, Koyasu S. 1999. Xid-like immunodeficiency in mice with disruption of the p85α subunit of phosphoinositide 3-kinase. Science 283:390–392.

Syukunami C, Shigeno C, Atsumi T, Ishizeki K, Suzuki F, Hiraki Y. 1996. Chondrogenic differentiation of clonal mouse embryonic cell line ATDC5 in vitro: Differentiation-dependent gene expression of parathyroid hormone (PTH)/PTH-related peptide receptor. J Cell Biol 133: 457–468.

Syukunami C, Ishizeki K, Atsumi T, Ohta Y, Suzuki F, Hiraki Y. 1997. Cellular hypertrophy and calcification of embryonal carcinoma-derived chondrogenic cell line ATDC5 in vitro. J Bone Miner Res 12:1174–1188.

Terauchi Y, Tsuji Y, Satoh S, Minoura H, Murakami K, Okuno A, Inukai K, Asano T, Kaburagi Y, Ueki K, Nakajima H, Hanafusa T, Matsuzawa Y, Sekihara H, Yin Y, Barrett JC, Oda H, Ishikawa T, Akanuma Y, Komuro I, Suzuki M, Yamamura K-I, Kodama T, Suzuki H, Koyasu S, Aizawa S, Tobe K, Fukui Y, Yazaki Y, Kadowaki T. 1999. Increased insulin sensitivity and hypoglycemia in mice lacking the p85α subunit of phosphoinositide 3-kinase. Nat Genet 21:230–235.

Toker A, Cantley LC. 1997. Signalling through the lipid products of phosphoinositide-3-OH kinase. Nature 387: 637–676.

Vortkamp A, Lee K, Lanske B, Segre GV, Kronenberg HM, Tabin CJ. 1996. Regulation of rate of cartilage differentiation by Indian hedgehog and PTH-related protein. Science 273:613–622.